RESEARCH ARTICLE

A molecular dynamic investigation of human rhinovirus 3c protease drug target: insights towards the design of potential inhibitors

Ndumiso M Buthelezi[1], Daniel G. Amoako[2, *], Anou M. Somboro[2], Ellisau Yakubu[1], Rene B. Khan[1], Hezekiel M. Kumalo[1, *]

[1]Discipline of Medical Biochemistry, School of Laboratory Medicine and Medical Science, [2]Biomedical Resource Unit, College of Health Sciences, University of KwaZulu-Natal, Durban, South Africa

Received: February 28, 2022; **accepted:** May 26, 2022.

The 3C protease is distinguished from most proteases due to the presence of cysteine nucleophile that plays an essential role in viral replication. This peculiar structure encompassed with its role in viral replication has promoted 3C protease as an interesting target for therapeutic agents in the treatment of diseases caused by human rhinovirus (HRV). However, the molecular mechanisms surrounding the chirality of inhibitors of HRV 3C protease remain unresolved. Herein using in silico techniques such molecular dynamic simulation and binding free estimations *via* molecular mechanics poisson–boltzmann surface area (MM/PBSA), we present a comprehensive molecular dynamics study of the comparison of two potent inhibitors, SG85 and rupintrivir, complexed with HRV-3C protease. The binding free energy studies revealed a higher binding affinity for SG85 of 58.853 kcal/mol than that for rupintrivir of 54.0873 kcal/mol and this was found to be in correlation with the experimental data. The energy decomposition analysis showed that residues Leu 127, Thr 142, Ser 144, Gly 145, Tyr 146, Cys 147, His 161, Val 162, Gly 163, Gly 164, Asn 165, and Phe 170 largely contributed to the binding of SG85, whereas His 40, Leu 127, and Gly 163 impacted the binding of rupintrivir. The results further showed that His 40, Glu 71, Leu 127, Cys 147, Gly 163, and Gyl 164 were crucial residues that played a key role in ligand-enzyme binding, and amongst these crucial residues, His 40, Glu 71, and Cys 147 appeared to be conserved in the active site of HRV-3C protease when bound by both inhibitors. These findings provided a comprehensive understanding of the dynamics and structural features and would serve as guidance in the design and development of potent novel inhibitors of HRV.

Keywords: 3C protease; rupintrivir; SG85; human rhinovirus; molecular dynamics; molecular mechanics/generalized born surface area.

[*]**Corresponding author:** Hezekiel M. Kumalo, Discipline of Medical Biochemistry, School of Laboratory Medicine and Medical Science, University of KwaZulu-Natal, Durban, South Africa. Phone: +27 031 260 7413. Email: KumaloH@ukzn.ac.za. Daniel G. Amoako, Biomedical Resource Unit, College of Health Sciences, University of KwaZulu-Natal, Durban, South Africa. Phone: +27 084 330 8957. Email: amoakodg@gmail.com.

Introduction

Human rhinovirus (HRV), also known as the causative agent of common cold [1, 2], is non-enveloped virus that contains a single-strand ribonucleic acid (ssRNA) genome enclosed in an icosahedral (20-sided) capsid [3]. It is estimated that 18.8 billion and 150 million people were infected with upper respiratory and lower respiratory infections, respectively [4]. The World Health Organization (WHO) estimates that HRV is responsible for nearly 2 million infant deaths, prompting the development of more effective medications [5].

HRV is divided into three types, RV-A, RV-B, and RV-C [6]. RV-C has just recently been discovered, and studies reveal that HRV 3C is the most

common HRV seen in hospitalized children [7]. HRV is a positive sense ssRNA virus of approximately 7,200 bp [8]. Upon infection, the positive-strand RNA genome of HRV 3C is translated into a large poly-protein essential for the production of new infectious virion and depends on two virally encoded proteases, 2A and 3C [9, 10]. The 3C protease plays an indispensable role in viral replication in proteolytic cleavage of large polyproteins to functional proteins and enzymes, which are structurally and enzymatically essential for viral RNA replication [11]. The enzyme possesses a strictly conserved catalytic active site, thus, making it an attractive target for therapeutic agents in the treatment of diseases caused by human rhinovirus [12, 13].

Rupintrivir (formerly AG7088) is an irreversible inhibitor of the human rhinovirus (HRV) 3C protease, which was discovered using structure-based drug design methodologies [14]. Clinical trials revealed that rupintrivir treatment was able to moderate the severity of illness and reduce the viral load in a human experimental HRV challenge trial, thus providing a proof of concept for the mechanism of 3C protease inhibition. It was later found that rupintrivir was not able to significantly affect virus replication or disease severity, and therefore, the further clinical development of rupintrivir ended abruptly [15].

SG85 is a peptidomimetics with Michael acceptor warheads permanently disable the protease by covalent binding to its catalytic site and is the most promising candidate [16]. SG85 is an efficient inhibitor of EV68 3C-protease and inhibits the replication of enteroviruses in cell-based assays [16].

It is believed that inhibition of picornavirus replication reduces the severity and shortens the duration of cold symptoms while rupintrivir is an irreversible inhibitor of HRV 3C protease and is regarded as the most potent novel peptidomimetic with inhibition activity against HRVs [17]. However, there is no evidence and comparison between these two inhibitors in terms of binding efficiency at molecular level. Hence, the molecular understanding of HRV-3C protease structure and ligand-binding mechanisms remains unclear. Molecular dynamic simulation is one of the useful tools that have the capacity to provide a concise understanding at atomic level of complex systems [18]. In recent years, different post-dynamics analyses such as root mean square fluctuation, principal component analysis, Mechanics/Generalized Born Surface Area, and dynamic cross-correlation analyses have been applied extensively in understanding the dynamics of biological complex systems at the atomic level. Therefore, molecular dynamic simulation (MD) analysis was employed in this work to study the binding of the two inhibitors with HRV-3C protease to provide understanding of molecular dynamics of HRV-3C protease complexed with SG85 and rupintrivir from a computational point of view. Furthermore, this study aimed at providing insight into the binding-landscape of the two inhibitors in HRV 3C protease by conducting a broad comparative MD analysis of the HRV 3C-Free, HRV 3C-SG85, and HRV 3C-Rupintrivir systems. The results of this study could serve as a cornerstone in drug design and developments of more potential drugs against HRV protease, which could lead the fight against the virus.

Materials and methods

System preparations

The X-ray crystal structure of human rhinovirus 3C protease bound to rupintrivir was extracted from Protein Data Bank (PDB) (www.rcsb.org) (PDB code: 5FX6) [19]. The Michael acceptor, SG85, crystal structure was complex with a crystal structure of corona virus HKU4 (PDB code: 2YNB) [20]. SG85 was removed and docked into the active site of the crystal structure of human rhinovirus 3C protease. This was done on the graphical user interface of UCSF Chimera version 1.15 (https://www.cgl.ucsf.edu/chimera/) (University of California San Francisco, San Francisco, CA, USA), where all non-standard residues irrelevant to the study such as ions, co-

factors, H_2O, and the corona virus HKU4 were removed. The missing residues were added by using a graphical user interface of molecular modeling tool of UCSF Chimera version 1.15 [21]. Ligand and receptor alterations as well as visualizations were conducted in Chimera and Avogadro software version 1.2.0 (University of Pittsburg, Pittsburgh, Pennsylvania, USA) (https://avogadro.cc/) [22].

System setup

The simulation setup was done by using Graphical Processing Unity (GPU) version of Amber 14 software package (University of California San Francisco, San Francisco, CA, USA) (https://ambermd.org) [23, 24]. The receptor and ligand were optimized by using the Amber 14 modules ANTECHAMBER and LEAP for 200 ns MD simulations [25]. Within the Amber 14, a FF14SB force field was used to parameterize the protein system [26, 27]. The systems were immersed in a box with TIP3P [28] water molecules at a distance of 10 Å. The system setup, minimizations, heating, and equilibration steps were thoroughly explained in our previous works [29, 30]. A total continuous MD simulation time of 200 ns was performed, and the trajectories were then saved for every 1 ps and analyzed. CPPTRAJ and Process TRAJectory (PTRAJ) modules [31] were used for analysis of Root Mean Square Deviation (RMSD), Root Mean Square Fluctuation (RMSF), Radius of Gyration (RoG), Dynamic Cross Correlation (DCC), and Principal Component Analysis (PCA). Origin data analysis tool (www.originlab.com) was used to plot while Chimera [21] was used for visualizations.

Binding energy calculations

The binding free-energy profiles of rupintrivir and SG85 bound to HRV 3C protease were computed by using the Molecular Mechanics/Generalized Born Surface Area (MM/GBSA) approach [32, 33]. From binding free energy, valuable insight into the association of the protein-ligand in a complex was obtained and was considered to be the end point energy calculation. The binding free energy was calculated by taking into account 1,000 snapshots from 200 ns trajectories.

The following set of equations described the calculation of the binding free energy:

$$\Delta G_{bind} = G_{complex} - G_{receptor} - G_{ligand} \quad (1)$$

$$\Delta G_{bind} = E_{MM} + G_{sol} - T\Delta S \quad (2)$$

$$E_{gas} = E_{int} + E_{vdw} + E_{ele} \quad (3)$$

$$G_{sol} = G_{GB/PB} + G_{SA} \quad (4)$$

$$G_{SA} = \gamma SASA \quad (5)$$

where ΔG_{bind} was the sum of the gas phase (E_{MM}) and solvation energy (G_{sol}) terms less the entropy ($T\Delta S$) term. $G_{complex}$ represented energy of the receptor ligand complex. $G_{receptor}$ and G_{ligand} represented energies of receptor and ligand, respectively. E_{gas} denoted gas-phase energy. E_{int} signified internal energy while E_{ele} and E_{vdw} represented the electrostatic and Van der Waals contributions, respectively. E_{gas} was the gas phase that elevated directly from the FF14SB force terms. G_{sol} denoted solvation free energy and could be decomposed into polar and nonpolar contribution states. The polar solvation contribution (G_{GB}) was determined by solving the GB equation, whereas the nonpolar solvation contribution (G_{SA}) was estimated from the solvent accessible surface area (SASA) that was determined by using a water probe radius of 1.4 Å. T and S corresponded to temperature and total solute entropy, respectively. γ was a constant. To determine the contribution of each of the amino acid towards total binding free energy profile between rupintrivir and SG85, a per-residue decomposition analysis of the interaction energy for each residue was carried out by using the MM/GBSA method.

Dynamic cross-correlation (DCC) analysis

The dynamic cross correlation (DCC) has been extensively applied to quantify the correlation coefficients of motions between atoms of a protein [34]. The CPPTRAJ module was used to calculate the residue-based fluctuations during the simulation [31]. DCC was represented by the following formula given below:

$$C_{ij} = \frac{<\Delta r_i.\Delta r_j>}{\left(<\Delta r_i^2><\Delta r_j^2>\right)^{1/2}}$$

where C_{ij} was the cross-correlation coefficient, which varied with a range of -1 to +1. A fully correlated and anti-correlated motion represented the upper and lower limits during the simulation, respectively. i and j represented the i^{th} and j^{th} residues and Δr_i and Δr_j symbolized displacement vectors corresponding to i^{th} and j^{th} residues, respectively. In this study, DCC calculations were carried out by considering the backbone C-α atomic fluctuations.

Principal component analysis (PCA)

Principal component analysis (PCA) is also referred as essential dynamics (ED) and is one of the utmost unconventional methods for trajectory analysis. PCA has proved to be powerful and robust and opens new opportunities to visualize and explore the dynamics of protein cavities [35, 36]. PCA describes the eigenvectors and eigenvalues, which represent the direction of motions and the amplitudes in those directions of the protein, respectively [37]. After stripping the ions and solvent of the 200 ns MD trajectories, PCA was performed on C-α atoms over 1,000 snapshots at a time interval of 100 ps by using the CPPTRAJ module in AMBER 14 in computing the first two principal components (PCA1 and PC2). The corresponding PCA scatter plots were generated by using Origin software (www.originlab.com).

Results and discussion

Root of mean square deviation (RMSD)

The mean root-mean-square deviation (RMSD) was plotted to identify the stability of studied enzyme-ligand complexes during the 200 ns MD trajectories. Figure 1 highlighted the RMSD of HRV 3C-Free, HRV 3C-SG85, and HRV 3C-Rupintrivir. Throughout the simulation, the three systems showed acceptable stability. In Figure 1, HRV 3C-Free maintained the highest average of 1.7643 ± 0.03972 Å comparing to HRV 3C-Rupintivir and HRV 3C-SG85 systems with an average RMSD of 1.2541 ± 0.1399 Å and 0.9714 ± 0.0826 Å, respectively. A drastic fluctuation at 150 ns was of significant note, though the system soon regained stability at 170 ns. However, following the analysis conducted, a stabilization and convergence of the systems, all the systems had fluctuations of less than < 2.5 Å.

Root mean square fluctuation (RMSF)

Proteins are bound to undergo structural fluctuations when subjected to physiological conditions. Relatively small and large structural fluctuations are directly related to protein functions that occur at a range of time scales, in this study, nanoseconds [38]. A RMSF plot in Figure 2 was used to analyze the amino acid fluctuations for all the HRV systems. In the current work, a similar trend in fluctuations was noticed in HRV 3C-Free, HRV 3C-Rupitrivir, and HRV 3C-SG85 with an average RMSF values of 0.7518 ± 0.3246 Å, 0.7144 ± 0.3328 Å, and 0.6098 ± 0.1981 Å, respectively. Hence, HRV 3C-Free system displayed more flexibility comparing to HRV 3C-Rupintrivir, and HRV 3C-SG85. The most significant change was observed in the active site residues in the regions 120-138 and 140-150 of the HRV 3C-Free enzyme and HRV 3C-Rupintrivir displayed higher fluctuations with reference to the HRV 3C-SG85. In addition, the proximal residues in the region 25-35 of the HRV 3C-Free exhibited higher fluctuations than that of both HRV 3C-Rupintrivir and HRV 3C-SG85. As evident in Figure 2, SG85 had reformed the overall protein flexibility comparing to Rupintrivir. Furthermore, Figure 2 gave the information about the β-hairpin in the active site residues in the regions 120-138 of all systems. It had been proposed that the β-hairpin acted as launch sites in initial events of protein folding [39]. Herein, the evolutions of the β-hairpin during a MD simulation for all conformations were examined and snapshots along the trajectories of MD simulations were shown in Figure 3.

During the simulation of the conformations, the β-hairpin on HRV 3C-Free system disappeared at

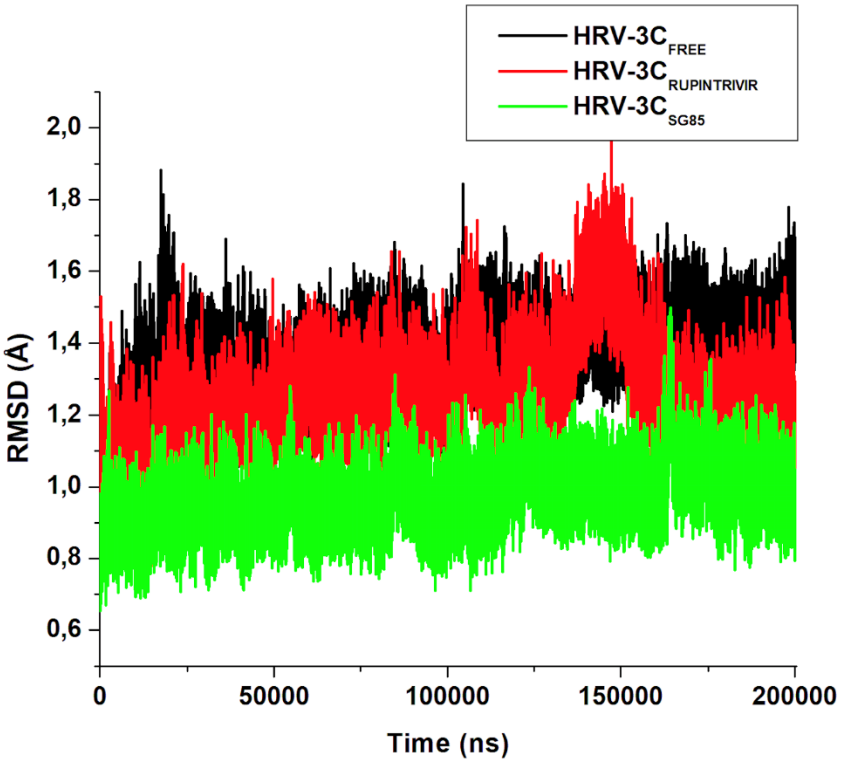

Figure 1. RMSD of minimized structures of HRV 3C-Free, HRV 3C-Rupintrivir, and HRV 3C-SG85 recorded over 200 ns MD simulation.

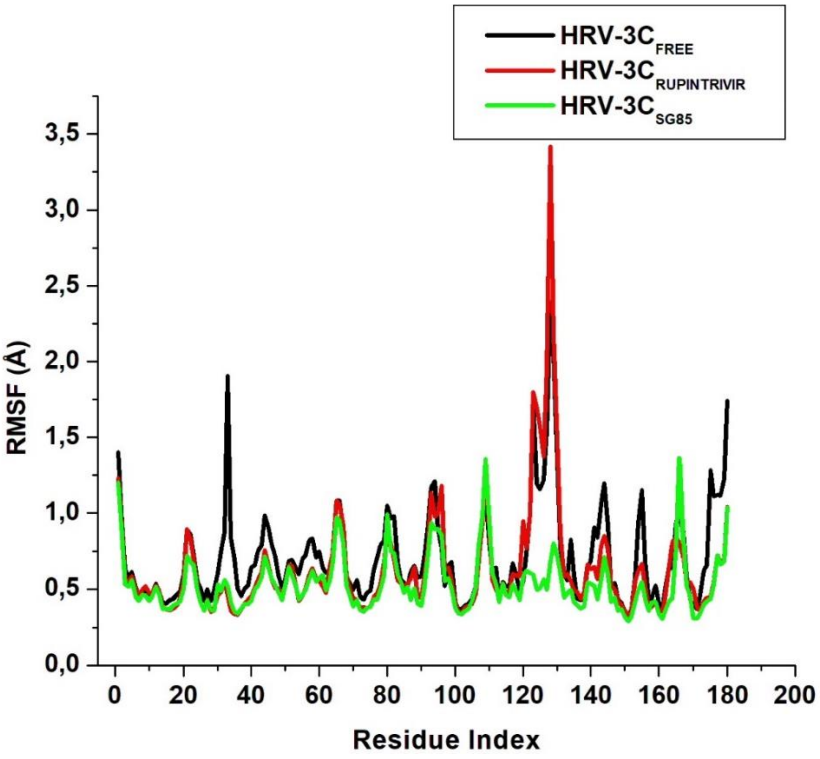

Figure 2. RMSF of minimized structures of HRV 3C-Free, HRV 3C-Rupintrivir, and HRV 3C-SG85 recorded over 200 ns MD simulation.

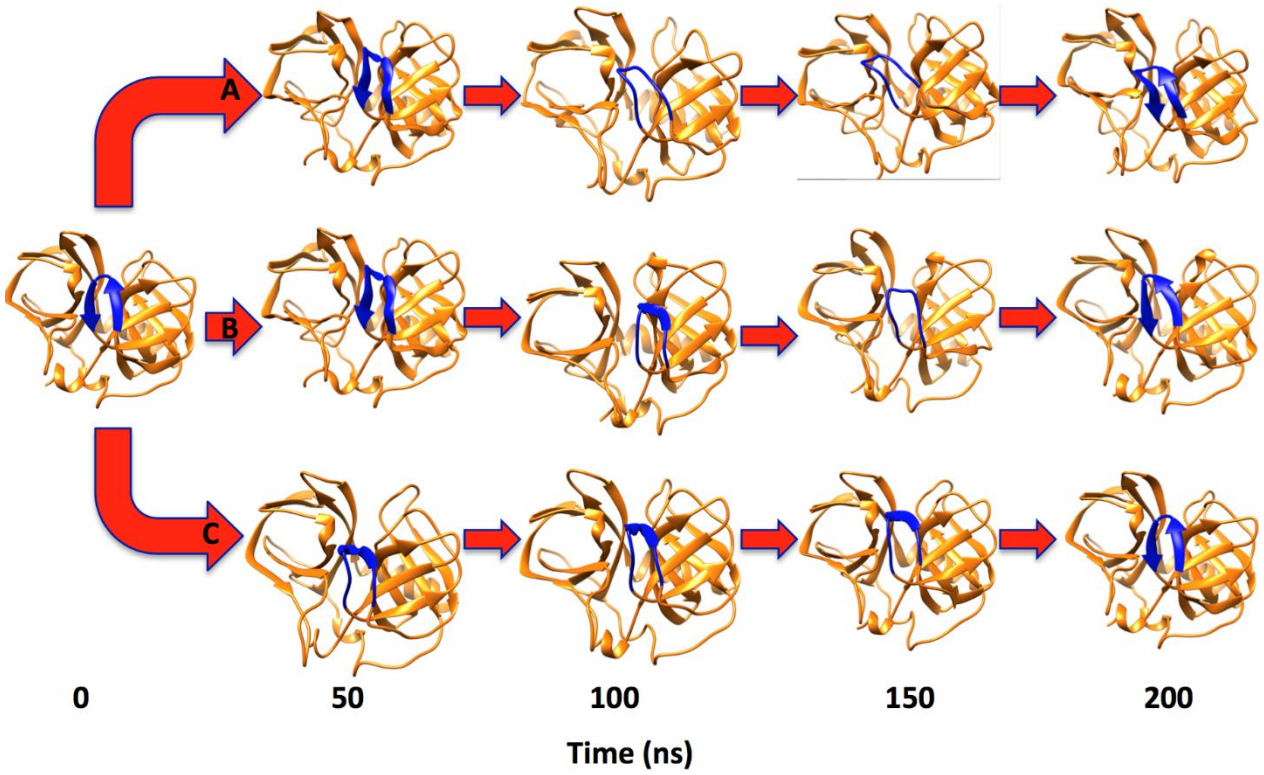

Figure 3. Snapshots of HRV 3C-Free (A), HRV 3C-Rupintrivir (B), and HRV 3C-SG85 (C) conformations captured at 50 ns intervals throughout a 200 ns MD simulation.

100 ns and 150 ns with an increase in loop length, whereas the β-hairpin on HRV 3C-Rupintrivir conformation disappeared at 150 ns with an increase in loop length (Figure 2). On the other hand, snapshots of HRV 3C-SG85 suggested a β-hairpin to be stable throughout a 200 ns MD simulation. Hence, these findings were correlated to those of RMSF presented herein, which justified a greater existence of fluctuations of HRV 3C-Free and HRV 3C-Rupintrivir comparing to HRV 3C-SG85 in the regions 120-138. Recent works suggested that the β-hairpin could form nucleation sites for protein folding. However, the molecular mechanisms by which proteins fold have not been yet fully understood [40–42]. Therefore, the findings presented herein could serve as basis in the understanding of the sequence and structural context of HRV β-hairpin. Experimental results had shown SG85 to be active against a wide range of HRV isolates suggesting that it had a higher affinity for the binding site than that of Rupintrivir [43]. We concluded from the results that location of SG85 in the active site led to a conformational rigidity and β-hairpin stability [16].

Radius of gyration (Rg)

Radius of gyration (Rg) was computed to measure the compactness of the protein structure as well as to provide insight into complex stability of the systems [44, 45]. An Rg plot in Figure 4 was used to analyze the overall protein dimensions of the HRV systems. From Figure 4, it was evident that the three systems shared close resemblance, which was explained by the similar alignment of the residues within the secondary and tertiary structures. HRV 3C-Free and HRV 3C-Rupintrivir displayed a slighter higher Rg than that of HRV 3C-SG85. These results were in accordance with RMSF, which justified a substantial increase in biomolecular flexibility of the HRV 3C-Free and HRV 3C-Rupintrivir when compared to the HRV 3C-SG85. This indicated that HRV possessed a rigid

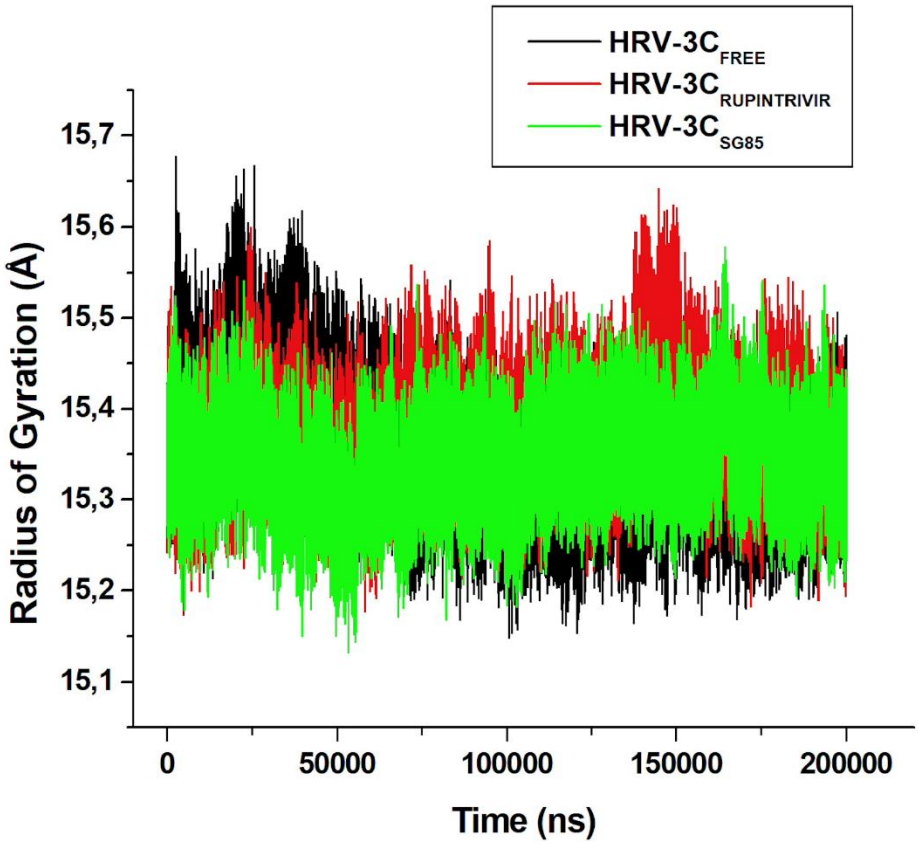

Figure 4. Rg of minimized structures of HRV 3C-Free, HRV 3C-Rupintrivir, and HRV 3C-SG85 recorded over 200 ns MD simulation.

structural stability when it was bound to SG85 as compared to. A theoretical explanation to this observation was that SG85 bound to the active site of HRV led to a conformational rigidity, which halted conformational flexibility of HRV.

Dynamic cross correlation (DCC) analysis

The dynamic cross correlation was applied to quantify the correlation coefficients of motions of the C-α atom fluctuations between atoms of a protein. The different correlation motion of the systems was analyzed. DCC plots presented in Figure 5 were interpreted based on the different colors with yellow to red indicating a strong correlation while blue to black indicated a strong anti-correlation of specific residue movements. Anti-correlated residual motion in Figure 5, for SG85, occurred between residues 50 – 70 relative to 110, while a strong correlated residual motion in case of rupintrivir occurred between 20 – 80 relative to each other. The correlation map displayed a strong correlation residual motion in the HRV 3C-Rupintrivir conformation, while the HRV 3C-SG85 conformation indicated a greater existence of negative correlated motions during simulation time. This was supported by the RMSF results, which also showed a strong interaction with residues comparing to HRV 3C-Rupintrivir.

Principal component analysis (PCA)

Figure 6 highlighted the dominant changes in motion across principal components of the HRV 3C-Free, HRV 3C-Rupintrivir, and HRV 3C-SG85. Principal component analysis (PCA) was used to characterize the conformational variations of SG85 and rupintrivir. PCA is a tool commonly used for conformational variations. The conformational motions of all the systems were plotted on the two principal components (PC1 *vs*. PC2) in order to gain a comprehensive understanding of the conformational changes in the systems. Figure 6 illustrated that SG85 (in

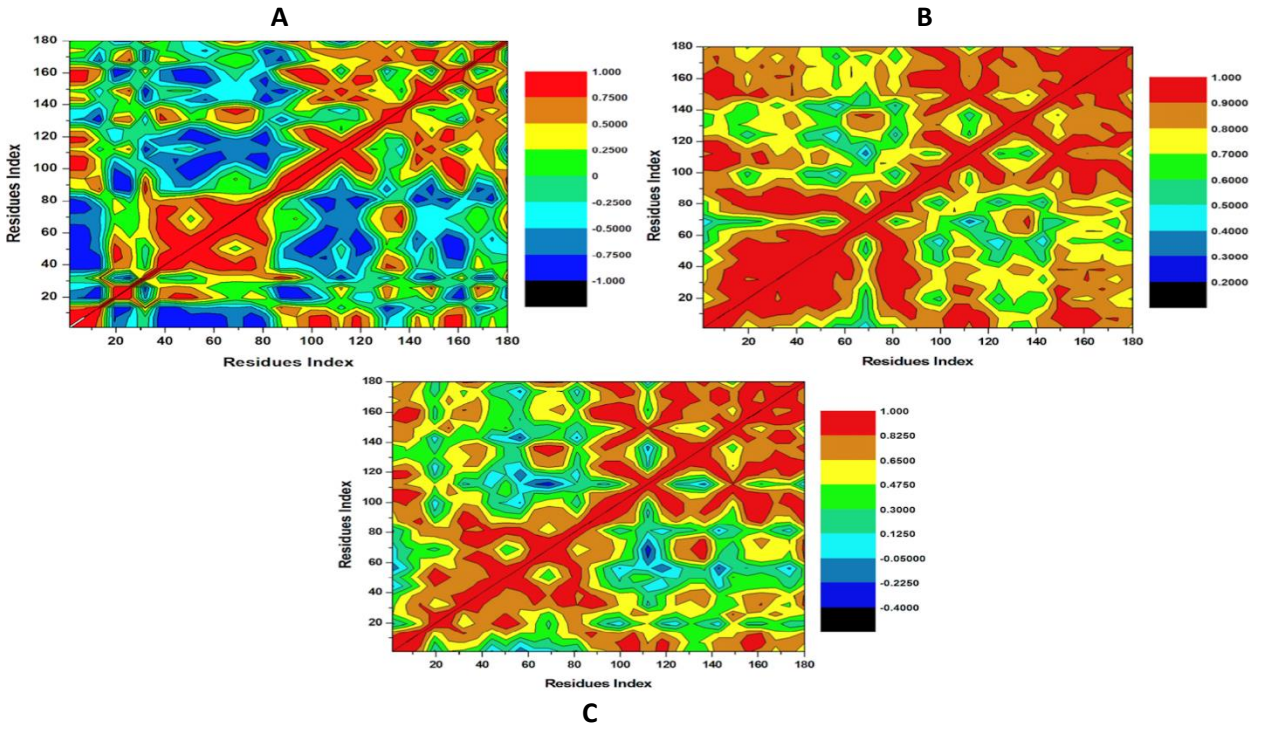

Figure 5. The dynamic cross correlation matrix analyses during the 200 ns simulation for the HRV 3C-Free (A), HRV 3C-Rupintrivir (B), and HRV 3C-SG85 (C).

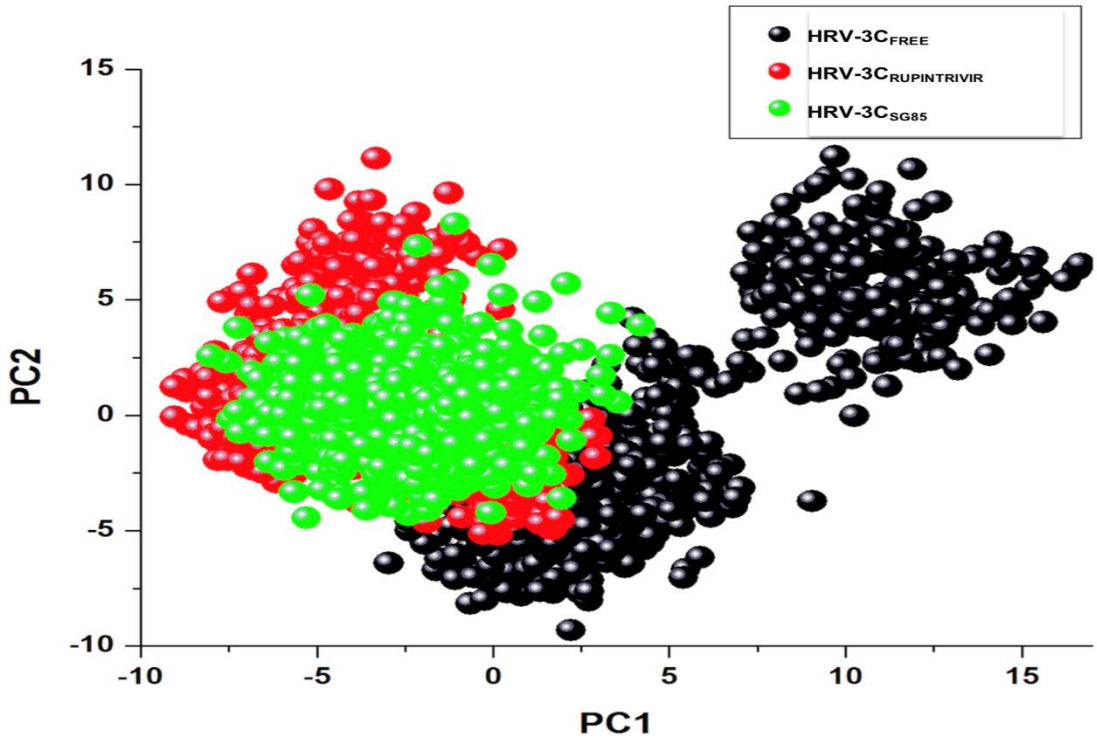

Figure 6. Projection of PC1 over PC2 for HRV 3C-Free, HRV 3C-Rupintrivir, and HRV 3C-SG85 conformations.

Table 1. MM/PBSA based on binding free energy profile of rupintrivir and SG85 bound with 3C protease.

Complexes	ΔG_{bind}	ΔE_{ele}	ΔE_{vdw}	ΔE_{gas}	ΔG_{sol}
Rupintrivir	-54.087	-47.236	-58.999	-106.236	52.149
SG85	-58.853	-207.650	-18.197	-100.047	25.203

Notes: ΔG_{bind}: binding energy; ΔE_{ele}: electrostatic; ΔE_{vdw}: van der waals; ΔE_{gas}: gas-phase energy; ΔE_{sol}: solvation energy.

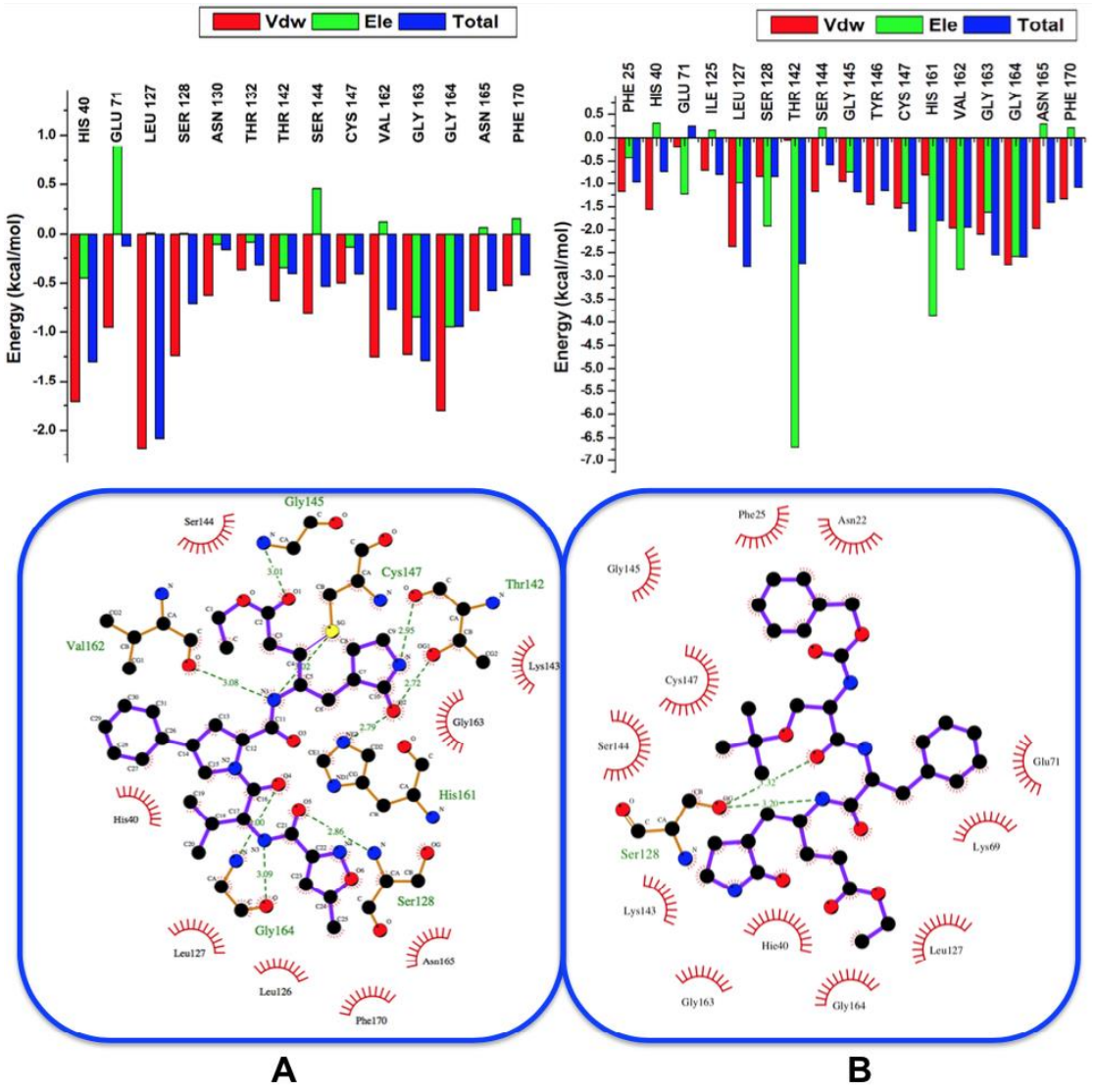

Figure 7. A diagrammatic representation of the per-residue graphs and 2D ligand interaction plots showing BFE contribution for rupintrivir (A) and SG85 (B) bound to HRV 3C.

black) occupied a larger space followed by Rupintrivir (in red) when compared to Free (in green). This implied that SG85 possessed a lower degree of flexibility enabling the HRV enzyme to bind easily comparing to Rupintrivir. As evident in Figures 2 and 3, the Free had more flexibility in comparison to Rupintrivir and SG85. From the evidence in Figure 6, a basic understanding of the dynamic behavior of the biological systems was attained.

Molecular mechanics poisson–boltzmann surface area (MM/PBSA) binding free energy calculation

The overall binding free energy for both SG85 and rupintrivir was calculated by using the MM/PBSA method. Per-residue energy decomposition was computed to gain insight to the ligand-residue interaction, and this was accomplished by 1,000 snapshots of the 200 ns simulation trajectories. As shown in Table 1, the binding free energy ($\Delta G_{binding}$) of SG85 and rupintrivir were -58.853 kcal/mol and -54.087 kcal/mol, respectively. The binding free energy of SG85 was higher by ~4 kcal/mol than that of rupintrivir, which further suggested that SG85 had a more intimate interaction with the active site residues comparing to rupintrivir. This was in great accordance with recent publications that had rated SG85 as the most potent inhibitor of HRV enzyme [16]. As evident from per-residue energy contribution plots in Figure 7, The larger residual energy contributions ($|\Delta G_{binding}| > - 1$) were Leu 127, Thr 142, Ser 144, Gly 145, Tyr 146, Cys 147, His 161, Val 162, Gly 163, Gly 164, Asn 165, Phe 170 for SG85, and His 40, Leu 127, Gly 163 for rupintrivir, respectively. However, in the case of SG85, Glu 71, a catalytic triad residue, showed an unfavorable energy contribution (+0.256 kcal/mol) and interestingly SG85 emerged as the potent inhibitor between the two. Moreover, both inhibitors interacted with the key residues His 40, Glu 71, and Cys 147. Thus, these results suggested that QSAR model should include these key residues for an efficient and effective drug design.

The current study highlighted the most important amino acids involved in inhibitor binding. The generated pharmacophore library was based only on highly contributing amino acid residues which was distinguished based on free binding energy contributions obtained from calculation from molecular dynamic (MD) simulations [46, 47]. We believed that the findings from this study could serve as a foundation towards the design of new inhibitors that would interact with catalytic triad residues to discover novel compounds to inhibit HRV by using a pharmacophore model.

Conclusion

Ligand-protein interaction and binding at molecular level is an imperative biological process. In this report, we provided insights into the binding mechanism of the rupintrivir and SG85 on 3C protease with the application of advance molecular dynamics simulation tools. It has been experimentally reported that SG85 is a potent inhibitor when compared to rupintrivir, but to this end, hence this comparative study was conducted by using various advanced MD simulation and post-analysis tools to gain understanding into the binding landscape and dynamic structural features associated with the binding of rupintrivir and SG85 on 3C protease. From the results obtained, SG85 induced a more stable protein structure thus suggesting a more intimate binding and interaction of SG85 with the 3C protease when compared to rupintrivir as seen from the RMSD, RMSF, RG, DCC, and PCA plots. The binding free energy calculation revealed a higher binding affinity for SG85 (-58.853 kcal/mol) than that for rupintrivir (-54.087 kcal/mol) and this was in correlation with the experimental data. This thus suggested that SG85 could be used as scaffold to design new inhibitors. The energy decomposition analysis showed that residues of Leu 127, Thr 142, Ser 144, Gly 145, Tyr 146, Cys 147, His 161, Val 162, Gly 163, Gly 164, Asn 165, Phe 170 largely contributed to the binding of SG85, whereas His 40, Leu 127 and Gly 163 largely contributed to the binding of rupintrivir. The energy decomposition revealed that His 40, Glu 71, Leu 127, Cys 147 Gly 163, and Gyl 164 were crucial residues that played a key role in ligand-enzyme binding; amongst these residues were residues of the conserved active site (His 40, Glu 71, and Cys 147). Therefore, from these results, we believe that the residue interactions and the binding free energy analysis must be considered for a pharmacophore model and structure-based design of novel and potent inhibitors of HRV.

Acknowledgements

Authors acknowledge School of Health Sciences, University of KwaZulu-Natal for financial assistance and the Center of High Performance Computing (CHPC) (www.chpc.ac.za) for computational facility.

References

1. Atkinson SK, Sadofsky LR, Morice AH. 2016. How does rhinovirus cause the common cold cough? BMJ Open Respir Res. 3(1):e000118.
2. Stobart CC, Nosek JM, Moore ML. 2017. Rhinovirus biology, antigenic diversity, and advancements in the design of a human rhinovirus vaccine. Front Microbiol. 8:2412.
3. Palmenberg AC, Gern JE. 2015. Classification and evolution of human rhinoviruses. Methods Mol Biol. 1221:1-10.
4. Lamborn IT, Jing H, Zhang Y, Drutman SB, Abbott JK, Munir S, *et al*. 2017. Recurrent rhinovirus infections in a child with inherited MDA5 deficiency. J Exp Med. 214(7):1949-1972.
5. Chadha M, Hirve S, Bancej C, Barr I, Baumeister E, Caetano B, *et al*. 2020. Human respiratory syncytial virus and influenza seasonality patterns-Early findings from the WHO global respiratory syncytial virus surveillance. Influenza Other Respir Viruses. 14(6):638-646.
6. Kerr SL, Mathew C, Ghildyal R. 2021. Rhinovirus and cell death. Viruses. 13(4):629.
7. L'Huillier AG, Kaiser L, Petty TJ, Kilowoko M, Kyungu E, Hongoa P, *et al*. 2015. Molecular epidemiology of human rhinoviruses and enteroviruses highlights their diversity in Sub-Saharan Africa. Viruses. 7(12):6412-6423.
8. Jacobs SE, Lamson DM, St. George K, Walsh TJ. 2013. Human rhinoviruses. Clin Microbiol Rev. 26(1):135-162.
9. Skorenski M, Sienczyk M. 2013. Viral proteases as targets for drug design. Curr Pharm Des. 19(6):1126–1153.
10. Flather D, Semler BL. 2015. Picornaviruses and nuclear functions: targeting a cellular compartment distinct from the replication site of a positive-strand RNA virus. Front Microbiol. 6:594.
11. Sun D, Chen S, Cheng A, Wang M. 2016. Roles of the picornaviral 3c proteinase in the viral life cycle and host cells. Viruses. 8(3):82.
12. Jensen LM, Walker EJ, Jans DA, Ghildyal R: Proteases of human rhinovirus: role in infection BT - rhinoviruses: methods and protocols. Edited by Jans DA, Ghildyal R. New York: Springer New York. 2015:129–141.
13. Ullah R, Shah MA, Tufail S, Ismat F, Imran M, Iqbal M, *et al*. 2016. Activity of the human rhinovirus 3c protease studied in various buffers, additives and detergents solutions for recombinant protein production. PLoS One. 11(4):e0153436.
14. Matthews DA, Dragovich PS, Webber SE, Fuhrman SA, Patick AK, Zalman LS, *et al*. 1999. Structure-assisted design of mechanism-based irreversible inhibitors of human rhinovirus 3C protease with potent antiviral activity against multiple rhinovirus serotypes. Proc Natl Acad Sci USA. 96(20):11000-11007.
15. Binford SL, Weady PT, Maldonado F, Brothers MA, Matthews DA, Patick AK. 2007. *In vitro* resistance study of rupintrivir, a novel inhibitor of human rhinovirus 3c protease. Antimicrob Agents Chemother. 51(12):4366–4373.
16. Lacroix C, George S, Leyssen P, Hilgenfeld R, Neyts J. 2015. The enterovirus 3c protease inhibitor sg85 efficiently blocks rhinovirus replication and is not cross-resistant with rupintrivir. Antimicrob Agents Chemother. 59(9):5814–5818.
17. Rocha-Pereira J, Nascimento MSJ, Ma Q, Hilgenfeld R, Neyts J, Jochmans D. 2014. The enterovirus protease inhibitor rupintrivir exerts cross-genotypic anti-norovirus activity and clears cells from the norovirus replicon. Antimicrob Agents Chemother. 58(8):4675–4681.
18. Chmiela S, Sauceda HE, Müller KR, Tkatchenko A. 2018. Towards exact molecular dynamics simulations with machine-learned force fields. Nat Commun. 9(1):3887.
19. Kawatkar SP, Gagnon M, Hoesch V, Tiong-Yip C, Johnson K, Ek M, *et al*. 2016. Design and structure–activity relationships of novel inhibitors of human rhinovirus 3C protease. Bioorg Med Chem Lett. 26(14):3248–3252.
20. Liu Y, Sheng J, Fokine A, Meng G, Shin WH, Long F, *et al*. 2015. Structure and inhibition of EV-D68, a virus that causes respiratory illness in children. Science. 347(6217):71-74.
21. Pettersen EF, Goddard TD, Huang CC, Couch GS, Greenblatt DM, Meng EC, *et al*. 2004. UCSF Chimera--a visualization system for exploratory research and analysis. J Comput Chem. 25(13):1605-1612.
22. Hanwell MD, Curtis DE, Lonie DC, Vandermeersch T, Zurek E, Hutchison GR. 2012. Avogadro: an advanced semantic chemical editor, visualization, and analysis platform. J Cheminform. 4(1):17.
23. Götz AW, Williamson MJ, Xu D, Poole D, Le Grand S, Walker RC. 2012. Routine microsecond molecular dynamics simulations with AMBER on GPUs. 1. Generalized Born. J Chem Theory Comput. 8(5):1542–1555.
24. Salomon-Ferrer R, Götz AW, Poole D, Le Grand S, Walker RC. 2013. Routine microsecond molecular dynamics simulations with AMBER on GPUs. 2. Explicit solvent particle mesh ewald. J Chem Theory Comput. 9(9):3878–3888.
25. Sprenger KG, Jaeger VW, Pfaendtner J. 2015. The general AMBER force field (GAFF) can accurately predict thermodynamic and transport properties of many ionic liquids. J Phys Chem B. 119(18):5882-5895.
26. Lindorff-Larsen K, Piana S, Palmo K, Maragakis P, Klepeis JL, Dror RO, *et al*. 2010. Improved side-chain torsion potentials for the Amber ff99SB protein force field. Proteins. 78(8):1950-1958.
27. Maier JA, Martinez C, Kasavajhala K, Wickstrom L, Hauser KE, Simmerling C. 2015. ff14SB: improving the accuracy of protein side chain and backbone parameters from ff99SB. J Chem Theory Comput. 11(8):3696–3713.
28. Jorgensen WL, Chandrasekhar J, Madura JD, Impey RW, Klein ML. 1983. Comparison of simple potential functions for simulating liquid water. J Chem Phys. 79(2):926–935.

29. Chetty S, Soliman MES. 2015. Possible allosteric binding site on Gyrase B, a key target for novel anti-TB drugs: Homology modelling and binding site identification using molecular dynamics simulation and binding free energy calculations. Med Chem Res. 24(5):2055–2074.
30. Kumalo HM, Soliman ME. 2016. A comparative molecular dynamics study on BACE1 and BACE2 flap flexibility. J Recept Signal Transduct. 36(5):505–514.
31. Roe DR, Cheatham TE 3rd. 2013. PTRAJ and CPPTRAJ: software for processing and analysis of molecular dynamics trajectory data. J Chem Theory Comput. 9(7):3084-3095.
32. Kollman PA, Massova I, Reyes C, Kuhn B, Huo S, Chong L, *et al*. 2000. Calculating structures and free energies of complex molecules: combining molecular mechanics and continuum models. Acc Chem Res. 33(12):889-897.
33. Massova I, Kollman PA. 2000. Combined molecular mechanical and continuum solvent approach (MM-PBSA/GBSA) to predict ligand binding. Perspect Drug Discov Des. 18(1):113–135.
34. Kasahara K, Mohan N, Fukuda I, Nakamura H. 2016. mDCC_tools: characterizing multi-modal atomic motions in molecular dynamics trajectories. Bioinformatics. 32(16):2531–2533.
35. Desdouits N, Nilges M, Blondel A. 2015. Principal component analysis reveals correlation of cavities evolution and functional motions in proteins. J Mol Graph Model. 55:13–24.
36. Martínez L. 2015. automatic identification of mobile and rigid substructures in molecular dynamics simulations and fractional structural fluctuation analysis. PLoS One. 10(3):e0119264.
37. Cocco S, Monasson R, Weigt M. 2013. From principal component to direct coupling analysis of coevolution in proteins: low-eigenvalue modes are needed for structure prediction. PLoS Comput Biol. 9(8):e1003176.
38. Fuglebakk E, Echave J, Reuter N. 2012. Measuring and comparing structural fluctuation patterns in large protein datasets. Bioinformatics. 28(19):2431–2440.
39. Blanco F, Ramírez-Alvarado M, Serrano L. 1998. Formation and stability of beta-hairpin structures in polypeptides. Curr Opin Struct Biol. 8:107–111.
40. Lee J, Shin S. 2001. Understanding β-hairpin formation by molecular dynamics simulations of unfolding. Biophys J. 81(5):2507–2516.
41. Diana D, De Rosa L, Palmieri M, Russomanno A, Russo L, La Rosa C, *et al*. 2015. Long range Trp-Trp interaction initiates the folding pathway of a pro-angiogenic β-hairpin peptide. Sci Rep. 5:16651.
42. Gao Y, Li Y, Mou L, Lin B, Zhang JZH, Mei Y. 2015. Correct folding of an α-helix and a β-hairpin using a polarized 2D torsional potential. Sci Rep. 5:10359.
43. Kaiser L, Crump CE, Hayden FG. 2000. *In vitro* activity of pleconaril and AG7088 against selected serotypes and clinical isolates of human rhinoviruses. Antiviral Res. 47(3):215–220.
44. Huang Y, Paul DR. 2007. Effect of molecular weight and temperature on physical aging of thin glassy poly(2,6-dimethyl-1,4-phenylene oxide) films. J Polym Sci Part B Polym Phys. 45(12):1390–1398.
45. Pan L, Patterson JC. 2013. Molecular dynamics study of Zn(aβ) and Zn(aβ)2. PLoS One. 8(9):e70681.
46. Kumalo HM, Soliman ME. 2016. Per-residue energy footprints-based pharmacophore modeling as an enhanced in silico approach in drug discovery: a case study on the identification of novel β-secretase1 (BACE1) inhibitors as anti-Alzheimer agents. Cell Mol Bioeng. 9:175–189.
47. Cele FN, Ramesh M, Soliman ME. 2016. Per-residue energy decomposition pharmacophore model to enhance virtual screening in drug discovery: a study for identification of reverse transcriptase inhibitors as potential anti-HIV agents. Drug Des Devel Ther. 10:1365-1377.